Chemical Physics Letters: X 3 (2019) 100030

Contents lists available at ScienceDirect

Chemical Physics Letters: X

journal homepage: www.journals.elsevier.com/chemical-physics-letters-x

The influence of the solvent's mass on the location of the dividing surface for a model Hamiltonian

R. Garcia-Meseguer[a], B.K. Carpenter[b,*], S. Wiggins[a,*]

[a] School of Mathematics, University of Bristol, University Walk, Clifton, Bristol BS8 1TW, United Kingdom
[b] School of Chemistry, Cardiff University, Cardiff CF10 3AT, United Kingdom

HIGHLIGHTS

- Dynamics of a model Hamiltonian representing solvent-solute repulsion are explored.
- Transition State dividing surface (DS) is located as a function of reduced mass of the model solvent.
- The DS can be very far from the saddle point on the PES when the reduced mass of the model solvent is large.
- The exact DS is sampled and trajectories initiated from it is compared with those from an approximate DS.
- The conventional TS can provide a very poor basis for calculating the reaction rate constant.

ARTICLE INFO

Keywords:
Dynamical systems
Dividing surface
Reactions in solution

2019 MSC:
00-01
99-00

ABSTRACT

The Transition State dividing surface is a key concept, not only for the precise calculation of the rate constant of a reaction, but also for the proper prediction of product ratios. The correct location of this surface is defined by the requirement that reactive trajectories do not recross it. In the case of reactions in solution the solvent plays an important role in the location of the dividing surface. In this paper we show with the aid of a model Hamiltonian that the effective mass of the solvent can dramatically change the location of the dividing surface.

1. Introduction

Finding the location of Dividing Surfaces (DSs) in chemical reactions has been the focus of many theoretical studies both for reactions in solution and in vacuum. Of particular interest is the DS, characterized as a hypersurface in phase space, which divides the reactants from products and has the property that trajectories cross it only once before entering a local minimum on the Potential Energy Surface (PES). The importance of this DS is that Transition State Theory calculates the rate constant as the flux of trajectories going through it. Of course, finding the exact DS is not an easy task for reactions of polyatomic molecules and could even be technically impossible for reactions in solutions.

There are several methodologies that try to approximate this DS, as discussed elsewhere [1–6]. These are, in principle, good approximations that rely solely on information obtained in configuration space and that, with the aid of corrections [7–10]. have delivered accurate results in the calculation of the reaction rate constant of many different chemical processes. However, as discussed in [11], not every effect can be explained with configuration-space models. One of these effects, which we have called the inertial barrier, arises when changes in shape of a reacting solute are resisted by the solvent because of a timescale mismatch between the solute dynamics (typically 100 fs for transit from a PES saddle point to the next local minimum, in vacuo) and solvent dynamics (typically 1–10 ps, and sometimes much longer, for relocation of solvent molecules in the first shell around the reacting solute) [12–20]. We have previously mentioned a 2 Degree of Freedom (DoF) model that mimics this effect in [11], and in this paper we explore its dynamics in detail.

The construction of the DS for 2 DoF systems using the Lyapunov family of unstable POs was presented in a series of papers by Pollak, Pechukas, and Child in the late 1970s to early 1980s [21–25]. The resulting Periodic Orbit Dividing Surface (PODS) is a hypersurface in phase space arising from the unstable PO. It has been shown to have the required no-recrossing properties described above. Of particular interest was the recognition that as the total energy of trajectories increased, the location of the PODS would change, and that, in general, its

* Corresponding authors.
E-mail addresses: carpenterb1@cardiff.ac.uk (B.K. Carpenter), S.Wiggins@bristol.ac.uk (S. Wiggins).

https://doi.org/10.1016/j.cpletx.2019.100030

Available online 22 April 2019

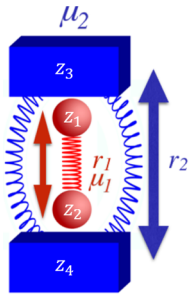

$$c = \begin{pmatrix} 321.904484 \\ -995.713452 \\ 1118.689573 \\ -537.856726 \\ 92.976121 \\ 1.0 \\ 1.0 \\ 0.01 \end{pmatrix} \qquad \begin{aligned} r_1 &= z_1 - z_2; \\ r_2 &= z_3 - z_4; \\ \mu_1 &= \frac{m_1}{2}; \\ \mu_2 &= \frac{m_2}{2} \end{aligned}$$

Fig. 1. Schematic representation (left) and definitions (right) of the model system used in our study.

projection onto the PES did not need to pass through the index one saddle point that is considered to be the location of the Transition Structure in many chemical models. In the present paper, we emphasize that it is not only energy which can cause the PODS to move, but at least in some models, its location may also be mass dependent. This feature is of particular relevance to the solvent-derived inertial barrier mentioned above.

The structure of this paper is as follows: in Section 2, we introduce a model potential energy function that approximates the interaction between a reactive system and a solvent and we calculate its Intrinsic Reaction Coordinate (IRC) for different values of the reduced mass of the solvent-like part of the model. In Section 3 we compute the PODSs and show how they vary with the reduced mass of the model solvent. In Section 4 we sample the DSs and compute transit times to the product well, and compare the results with those obtained from an approximate DS located at the PES saddle point. Finally, in Section 4 we discuss the results obtained and the conclusions extracted from them.

2. Potential energy surface

Our model potential (see Fig. 1) consists of a one-dimensional double well oscillator that represents the reactive system, coupled to a one-dimensional harmonic oscillator representing the bath. The only coupling between the two oscillators is a Lennard-Jones-like repulsion potential term. Consequently, this model is appropriate only for non-polar systems; our concern here is the consequence of non-bonded interactions between solvent and solute, not the more commonly studied polar interactions.

The Hamiltonian that describes the system is as follows:

$$H(\mathbf{x}) = H(\mathbf{r}, \mathbf{p}) = \frac{p_1^2}{2\mu_1} + \frac{p_2^2}{2\mu_2} + \sum_{j=1}^{5} c_j r_1^{j-1} + c_6(c_7 - r_2)^2 + \frac{c_8}{(r_2 - r_1)^{12}} \tag{1}$$

where the subscripts 1 and 2 refer to the reactive system and bath oscillators respectively; $r = (r_1, r_2)$ is the position of the two oscillators and $p = (p_1, p_2)$ represents the conjugate momenta. The reduced mass of each oscillator is represented by μ, and c are coefficients whose values are listed in Fig. 1. The potential energy can be divided between $\sum_{j=1}^{5} c_j r_1^{j-1}$ as the potential of the reactive system, $V_2 = c_6(c_7 - r_2)^2$ as the potential of the bath and $V_{int} = c_8(r_2 - r_1)^{-12}$ as the interaction between the two; hence $V = V_1 + V_1 + V_{int}$. The potential of the reactant, shown in Fig. 2, is chosen to have a minimum at $r_1 = 1.0$ and a second one at $r_1 = 2.0$, with respective potential energies $V_1 = 0.0$ and $V_1 = -10$. The maximum energy is at $r_1 = 1.33867$ and $V_1 = 2.0$. The full potential, shown in Fig. 2, has a saddle point at $r_1 = 1.36561$ and $r_2 = 2.161769$ at $V = 3.47291$. The "reactant" minimum occurs at $r_1 = 0.98779$, $r_2 = 1.80661$, $V = 0.77040$. The "product" minimum occurs at $r_1 = 1.98517$, $r_2 = 2.75642$, $V = -6.66284$.

For all of the following calculations, the reduced mass of the reactive system (μ_1) is set to a value of 1. The reduced mass of the bath (μ_2) is given values of 0.1, 1, 10 or 100. We begin by examining the Intrinsic Reaction Coordinates (IRCs), which are the steepest-descent paths down from the saddle point, in mass-weighted coordinates (see Fig. 3). As can be seen, at the lowest reduced mass for the bath oscillator, the IRC looks like a "normal" minimum-energy reaction path from one well to the other, through the saddle point. However, as the reduced mass of the bath oscillator is increased, it is apparent that system and bath contributions to the IRC are separating, until at $\mu_2 = 100$, they look almost completely decoupled.

Interestingly, though, despite the very different appearances of the IRCs, the potential energy profiles plotted along the IRCs, but expressed only as a function of r_1, look very similar to each other and, in relative-energy terms, quite similar to the system-only potential in Fig. 2 (see Fig. 3). In other words, the differences in system behavior as a function of μ_2 would be masked if one looked only at the evolution of the potential as a function of r_1.

3. Periodic orbit dividing surface

One of the reasons for choosing this system was the relative ease on computing the periodic orbits that define the PODSs. These calculations (and all the ones that will follow) were done at an energy of 3.691966889, i.e. slightly above the energy of the saddle point.

In order to understand the properties of the trajectories that depart from the DS we need to sample its points in phase space. The procedure, applicable to a 2 DoF Hamiltonian system, selects points on a 2D surface with fixed total energy (E), where the periodic orbit forms the one dimensional boundary of the DS. The algorithm is as described in [26,27]:

1. Locate an unstable PO.
2. Project the unstable PO into configuration space, which gives a curve in configuration space.
3. Choose points on the curve (x_i, y_i) for $i = 1, N$, where N is the desired number of points. The points are spaced uniformly according to distance along the PO.
4. For each point (x_i, y_i) determine $p_{x_{max},i}$ by solving for .

$$H(x_i, y_i, p_x, 0) = \frac{p_x^2}{2\mu_x} + V(x_i, y_i) = E \tag{2}$$

5. Note that solution of this equation requires $E - V(x_i, y_i) \geqslant 0$, and there will be two solutions, $\pm p_{x_{max},i}$.
6. For each point (x_i, y_i) choose points p_{x_j} for $j = 1, K$, with $p_{x_1} = -p_{x_{max},i}$ and $p_{x_K} = p_{x_{max},i}$ and solve the equation $H(x_i, y_i, p_x, p_y) = E$ to obtain p_y.

The geometrical structure of the DS sampled in this manner is a one parameter family of circles. The parameter defining the family is given by the distance along the projection of the PO onto the configuration space from Steps 1–3 in the algorithm above, and the momentum-space circles are given by the following equation obtained from the Hamiltonian:

$$\frac{p_x^2}{2\mu_x} + \frac{p_y^2}{2\mu_y} = E - V(x_i, y_i) \tag{3}$$

The geometry of this one parameter family of circles depends on the nature of the projection of the PO into configuration space. In this particular case the PO projections are arcs where a configuration space point on the projection of the PO moves back and forth along the arc. This means that the endpoints of the arc are turning points with $p_x = p_y = 0$, where the circles defined by Eq. (3) shrink to points. This implies that the geometry of the one parameter family of circles defines a 2D sphere (see Fig. 4 bottom).

In order to follow steps 1 and 2 of the sampling algorithm, it was necessary to fit functions to the POs. These functions are expressed as

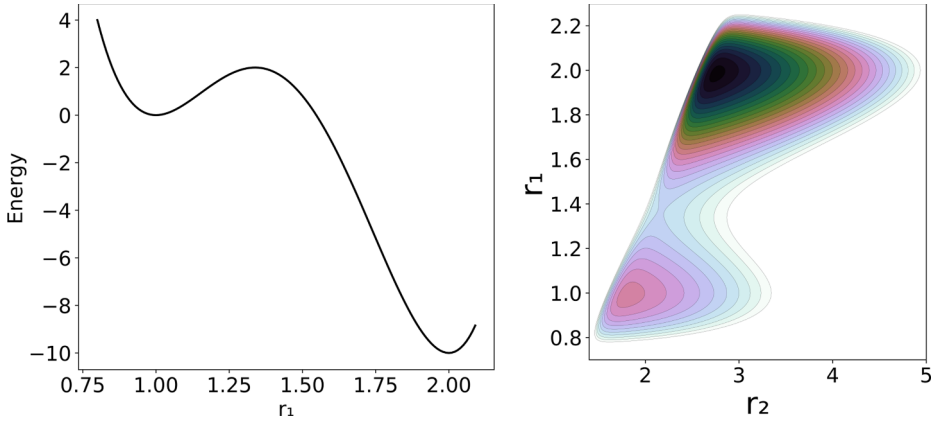

Fig. 2. (Left) Reactive system's potential energy profile. (Right) Contours of the full potential energy surface. The contours are depicted in the $-7 \leqslant V \leqslant 6$ interval.

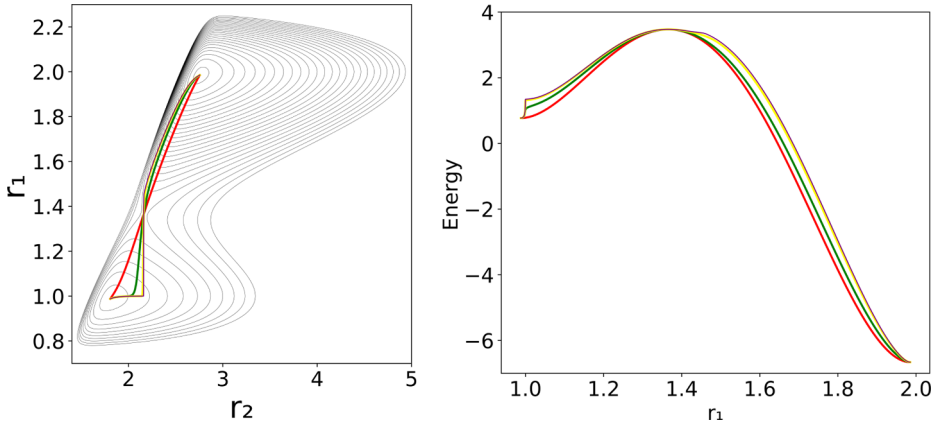

Fig. 3. (Left) Intrinsic reaction coordinates for various values of μ_2. (Right) Plots of the potential energy along each of the IRCs shown in (Left). The color correspondence is the following: 0.1 is red, 1 is green, 10 is yellow and 100 is purple. (For interpretation of the references to colour in this figure legend, the reader is referred to the web version of this article.)

$r_2 = f(r_1)$. Also, by the chain rule:

$$\frac{dr_2}{dt} = \frac{df}{dr_1}\frac{dr_1}{dt} \tag{4}$$

Hence the fitting function must satisfy the condition that:

$$\frac{p_2}{\mu_2} = \frac{df}{dr_1}\frac{p_1}{\mu_1} \tag{5}$$

and so the parameters of the functions were optimized in order to fit positions and momenta simultaneously. Each fitting function was a sum of exponentials:

$$r_2 = c_0 + \sum_{i=1}^{5} c_{2i-1} e^{-2i(r_1-b)} \tag{6}$$

In Fig. 4 (top) we can see the projection of the calculated PODSs in configuration space. Fig. 4 also includes two approximations to the DS explained in the caption and shows how the three of them respond as μ_2 changes. It can be seen that, for low reduced masses, the approximate DSs are close to the PODS. That is because the bath can rapidly adapt to the position of the reactive system. However, as μ_2 increases the PODS starts to curve and to displace from the approximate DSs, moving closer to the product well.

From the sampled trajectories we can measure the time taken to reach a determined region (transit time), in this case the PES minimum identified as the product well. Then we can perform the same calculation but with trajectories starting on the DS defined only with r_1 (the blue line in Fig. 4). The blue line corresponds to the common choice for solution phase reactions of assigning the transition state location to the PES saddle point, and assuming that the reaction coordinate is entirely determined by the solute. Fig. 5 is a representation in phase space of the transit times of trajectories that start on the true and approximate dividing surfaces with different initial $p_\perp$, the momentum normal to the dividing surface. The transit times (calculated as the time for r_1 to reach a value greater than that for product minimum) show brighter colors in Fig. 5 as the transit time increases. The expected results for a DS is that trajectories starting with negative momenta normal to the dividing surface ($p_\perp < 0$), i.e. directed to the reactant well, would take longer to reach the product well than those that start with positive momenta. This is clearly the case for the PODS as can be seen in Fig. 5, where $p_\perp = 0$ (which corresponds to the PO) provides an exact line of demarcation in the transit times. By contrast, the approximate DS shows long and short transit times on both sides of $p_1 = 0$. It is interesting to note that those areas where the transit times are long for $p_1 > 0$ or short for $p_1 < 0$ correspond to recrossing of trajectories, and that the amount of recrossing gets larger as μ_2 increases. Thus, the approximate DS becomes a poorer and poorer choice for the transition state as the mass of the bath oscillator increases.

The brighter colored bands visible on the reactant sides ($p_\perp < 0$) in Fig. 5 are associated with the many periodic orbits located in the reactant well. Trajectories that approach these POs can spend a long time before finally crossing over to the product well.

4. Conclusions

We have studied the effect of the mass in the location of the dividing surface on a model representing the interaction between a bath and a

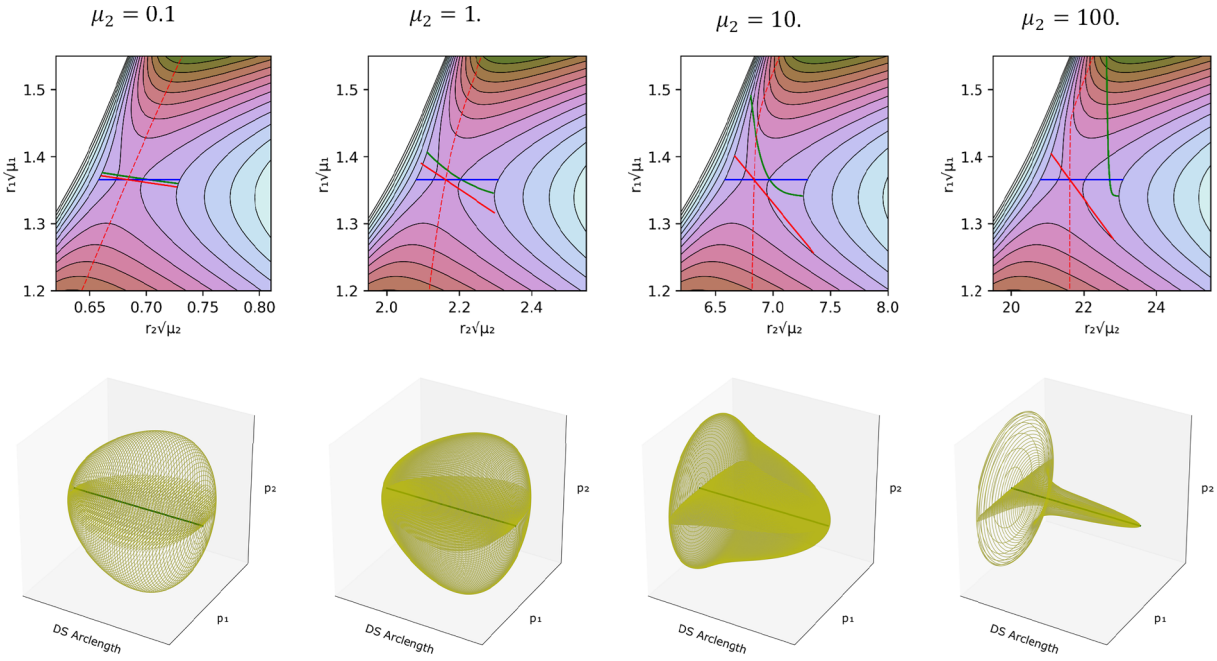

Fig. 4. (Top) Close-up of the PES of the full system, near the saddle point region at different reduced masses of the bath. Each of the axis scales were weighted by the square root of its coordinate mass. The dashed red line is the intrinsic reaction coordinate (IRC). The blue line is DS if one assumes that the reaction coordinate is r_1. The red line is the DS projection at the saddle point, which is locally orthogonal to the IRC (It does not look orthogonal because of the choice of axis scales). The green line is the projection of the PO that defines the Dividing surface. (Bottom) Schematic representation of the DS's geometrical structure for the different reduced masses. The yellow structure represents the possible momenta depending of the location in the DS. (For interpretation of the references to colour in this figure legend, the reader is referred to the web version of this article.)

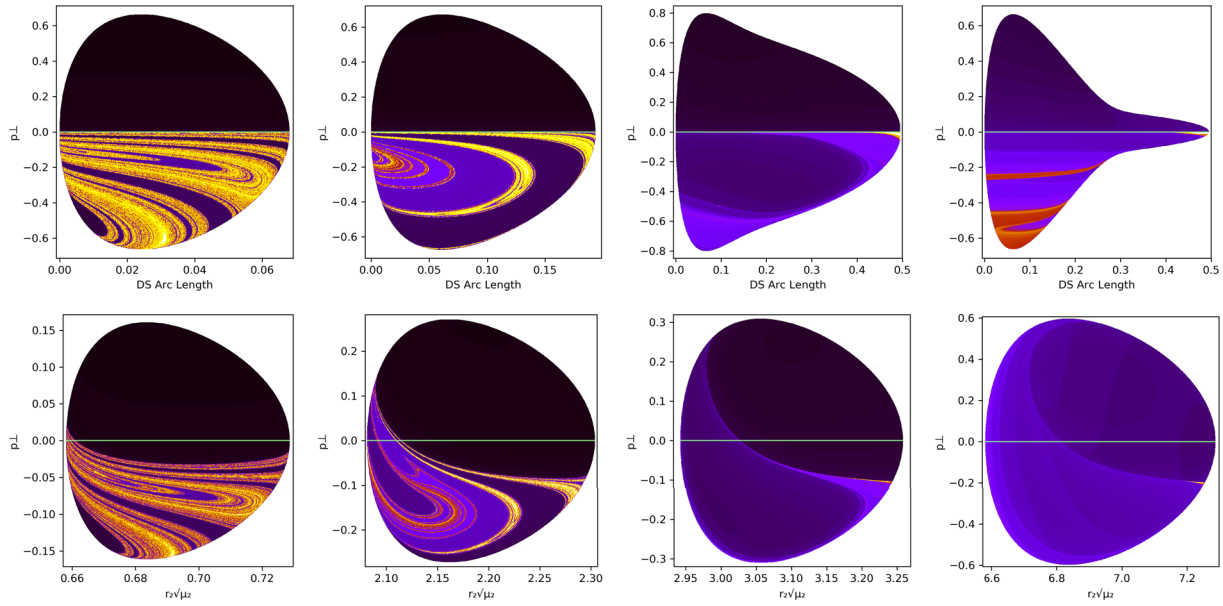

Fig. 5. A comparison of trajectory transit times from the DS to the product. (Top) Being the PODS (green DS in Fig. 4) and (Bottom) the DS conventional definition of the TS (blue DS in Fig. 4). The color scale goes from dark colors for short times to brighter colors for long times. The quantity $p_{\perp}$ is the momentum perpendicular to the dividing surface, with a positive sign being in the direction of the product. (For interpretation of the references to colour in this figure legend, the reader is referred to the web version of this article.)

reactive system. By calculating the PODSs we have been able to demonstrate that, as expected, they comply with the nonrecrossing requirement and to see how the dividing surface changes with the mass of the bath relative to the reactive system. These PODSs have shown that as the mass of the bath increases the actual dividing surface moves further away from the saddle point and also becomes more curved.

Although this simple model is obviously not representative of any real chemical reaction, we believe that it nonetheless provides useful insights for reactions in solution. In particular, when reacting solutes undergo changes in shape that require significant relocation of solvent molecules, the solvent may provide resistance to the reaction. For typical polyatomic organic solvents, it may be that several solvent molecules have to move in order to accommodate the requirements of the reacting solute, and under such circumstances the solvent-induced barrier to reaction may be particularly significant. As Bunker recognized many years ago [12] this effect shows up in the simulation as

a high effective mass for the solvent, and is represented in the present model by large values of μ_2. Common concerns in the modelling of solvent effects are to account for Coulombic interactions, i.e. polar effects. We have emphasized that our model does not seek to do that, and so is obviously incomplete. However, we believe that models which simulate only polar effects, as happens for some dielectric continuum models, are also incomplete. In fact, any models that describe solvent effects solely through changes in the potential energy part of the Hamiltonian will be unable to capture the effects that we have described here, which are consequences of changes in the kinetic energy part of the Hamiltonian.

Appendix A. Fitting Values

See Tables A.1 and A.2.

Table A.1
Coefficients used in Eq. (1) to define the shape of the Hamiltonian.

c_1	c_2	c_3	c_4
321.904484	−995.713452	1118.689573	−537.856726
c_5	c_6	c_7	c_8
92.976121	1.0	1.0	0.01

Table A.2
Coefficients used in Eq. (6) to fit the PODSs for each value of the reduced mass of the bath oscillator (μ_2).

μ_2	c_0	c_1	c_2
0.1	0.094165263108873	0.0160670338096018	65.5958200099274
1.0	1.84315847028138	0.00758954748486114	174.709820765531
10.0	5.98147469345274	0.105815259562613	409.082666681712
100.0	22.5611517645439	0.105015550264872	2364.74381214317
μ_2	c_3	c_4	c_5
0.1	0.617134920839315	5.94718114192171	0.0
1.0	0.0598940636386768	49.6008107125315	0.38366220493012
10.0	0.118183618431188	85.251388833634	0.158766384155483
100.0	0.0550009000221773	323.624788505891	0.0455268005566065
μ_2	c_6	c_7	c_8
0.1	0.0	0.0	0.0
1.0	6.05010733708722	0.0	0.0
10.0	19.0551458932095	0.783315335293556	0.622145175569231
100.0	82.7970050172418	0.0571491383435566	21.1545809216056
μ_2	c_9	c_{10}	b
0.1	0.0	0.0	1.36002047343
1.0	0.0	0.0	1.345715931855
10.0	0.105074746223228	0.198536432832936	1.34150785722358
100.0	0.115809707329263	2.8693949919629	1.34137751

Declaration of interests

The authors declare that they have no known competing financial interests.

Acknowledgements

The authors acknowledge the support of EPSRC Grant No. EP/P021123/1 and Office of Naval Research (Grant No. N00014-01-1-0769).

References

[1] J.L. Bao, D.G. Truhlar, Variational transition state theory: theoretical framework and recent developments, Chem. Soc. Rev. 46 (24) (2017) 7548–7596, https://doi.org/10.1039/C7CS00602K.
[2] D.G. Truhlar, B.C. Garrett, Variational transition-state theory, Acc. Chem. Res. 13 (12) (1980) 440–448, https://doi.org/10.1021/ar50156a002.
[3] P. Pechukas, Transition state theory, Ann. Rev. Phys. Chem. 32 (1) (1981) 159–177, https://doi.org/10.1146/annurev.pc.32.100181.001111 <https://www.annualreviews.org/doi/abs/10.1146/annurev.pc.32.100181.001111> .
[4] C.J. Cramer, D.G. Truhlar, Implicit solvation models: equilibria, structure, spectra, and dynamics, Chem. Rev. 99 (8) (1999) 2161–2200, https://doi.org/10.1021/cr960149m.
[5] C.J. Cramer, D.G. Truhlar, A universal approach to solvation modeling, Acc. Chem. Res. 41 (6) (2008) 760–768, https://doi.org/10.1021/ar800019z.
[6] J.L. Rivail, D. Rinaldi, Liquid-state quantum chemistry: computational applications of the polarizable continuum models, in: J. Leszczynski (Ed.), Computational Chemistry: Reviews of Current Trends, World Scientific, New York, 2011, pp. 139–174. doi:10.1142/9789812830364_0004 <https://www.worldscientific.com/doi/abs/10.1142/9789812830364_0004> .
[7] R.F. Grote, J.T. Hynes, The stable states picture of chemical reactions. ii. rate

constants for condensed and gas phase reaction models, J. Chem. Phys. 73 (6) (1980) 2715–2732.
[8] J.T. Hynes, Crossing the transition state in solution, in: O. Tapia, J. Bertrn (Eds.), Solvent Effects and Chemical Reactivity, Springer, Netherlands, Dordrecht, 2002, pp. 231–258, , https://doi.org/10.1007/0-306-46931-6_5.
[9] J.T. Hynes, The Theory of Chemical Reaction Dynamics, vol. 4, CRC Press, Fla, 1985.
[10] G. van der Zwan, J.T. Hynes, Dynamical polar solvent effects on solution reactions: a simple continuum model, J. Chem. Phys. 76 (6) (1982) 2993–3001, https://doi.org/10.1063/1.443392 <https://aip.scitation.org/doi/abs/10.1063/1.443392> .
[11] R. Garcia-Meseguer, B. Carpenter, Re-evaluating the transition state for reactions in solution, Eur. J. Org. Chem. 2019 (2–3) (2018) 254–266, https://doi.org/10.1002/ejoc.201800841 <https://onlinelibrary.wiley.com/doi/abs/10.1002/ejoc.201800841> .
[12] D.L. Bunker, B.S. Jacobson, Photolytic cage effect. monte-carlo experiments, J. Am. Chem. Soc. 94 (6) (1972) 1843–1848, https://doi.org/10.1021/ja00761a009.
[13] M.L. Horng, J.A. Gardecki, A. Papazyan, M. Maroncelli, Subpicosecond measurements of polar solvation dynamics: coumarin 153 revisited, J. Phys. Chem. 99 (48) (1995) 17311–17337, https://doi.org/10.1021/j100048a004.
[14] A.A. Deniz, B. Li, K.S. Peters, Role of polarization caging in the sn1 reaction of diphenylmethyl chloride: a picosecond kinetic study, J. Phys. Chem. 99 (32) (1995) 12209–12213, https://doi.org/10.1021/j100032a024.
[15] S.L. Chang, T.-M. Wu, A possible nonpolar solvation mechanism at an intermediate time scale: the solvent-cage expansion, Chem. Phys. Lett. 324 (5) (2000) 381–388, https://doi.org/10.1016/S0009-2614(00)00686-2 <http://www.sciencedirect.com/science/article/pii/S0009261400006862> .
[16] P. Larrgaray, A. Cavina, M. Chergui, Ultrafast solvent response upon a change of the solute size in non-polar supercritical fluids, Chem. Phys. 308 (1) (2005) 13–25, https://doi.org/10.1016/j.chemphys.2004.07.047 <http://www.sciencedirect.com/science/article/pii/S0301010404003970> .
[17] J.M. Anna, K.J. Kubarych, Watching solvent friction impede ultrafast barrier crossings: a direct test of kramers theory, J. Chem. Phys. 133 (17) (2010) 174506, https://doi.org/10.1063/1.3492724 <https://aip.scitation.org/doi/abs/10.1063/1.3492724> .
[18] J. Clark, T. Nelson, S. Tretiak, G. Cirmi, G. Lanzani, Femtosecond torsional relaxation, Nat. Phys. 8 (2012) 225, https://doi.org/10.1038/nphys2210 <https://www.nature.com/articles/nphys2210#supplementary-information> .
[19] S. Thallmair, M. Kowalewski, J.P.P. Zauleck, M.K. Roos, R. de Vivie-Riedle, Quantum dynamics of a photochemical bond cleavage influenced by the solvent environment: A dynamic continuum approach, J. Phys. Chem. Lett. 5 (20) (2014) 3480–3485, https://doi.org/10.1021/jz501718t.
[20] B.K. Carpenter, J.N. Harvey, D.R. Glowacki, Prediction of enhanced solvent-induced enantioselectivity for a ring opening with a bifurcating reaction path, Phys. Chem. Chem. Phys. 17 (13) (2015) 8372–8381, https://doi.org/10.1039/C4CP05078A.
[21] P. Pechukas, E. Pollak, Trapped trajectories at the boundary of reactivity bands in molecular collisions, J. Chem. Phys. 67 (12) (1977) 5976–5977, https://doi.org/10.1063/1.434777 <https://aip.scitation.org/doi/abs/10.1063/1.434777> .
[22] E. Pollak, P. Pechukas, Transition states, trapped trajectories, and classical bound states embedded in the continuum, J. Chem. Phys. 69 (3) (1978) 1218–1226, https://doi.org/10.1063/1.436658 <https://aip.scitation.org/doi/abs/10.1063/1.436658> .
[23] P. Pechukas, E. Pollak, Classical transition state theory is exact if the transition state is unique, J. Chem. Phys. 71 (5) (1979) 2062–2068, https://doi.org/10.1063/1.438575 <https://aip.scitation.org/doi/abs/10.1063/1.438575> .
[24] E. Pollak, M.S. Child, P. Pechukas, Classical transition state theory: a lower bound to the reaction probability, J. Chem. Phys. 72 (3) (1980) 1669–1678, https://doi.org/10.1063/1.439276 <https://aip.scitation.org/doi/abs/10.1063/1.439276> .
[25] P. Pechukas, Recent developments in transition state theory, Ber. Bunsen-Ges. Phys. Chem. 86 (5) (1982) 372–378, https://doi.org/10.1002/bbpc.19820860509 <https://onlinelibrary.wiley.com/doi/abs/10.1002/bbpc.19820860509> .
[26] F.A.L. Mauguiere, P. Collins, Z.C. Kramer, B.K. Carpenter, G.S. Ezra, S.C. Farantos, S. Wiggins, Phase space barriers and dividing surfaces in the absence of critical points of the potential energy: Application to roaming in ozone, J. Chem. Phys. 144 (5) (2016) 054107, https://doi.org/10.1063/1.4940798.
[27] G.S. Ezra, S. Wiggins, Sampling phase space dividing surfaces constructed from normally hyperbolic invariant manifolds (NHIMs), J. Phys. Chem. A 122 (42) (2018) 8354–8362.